Stabilizing quantum simulations of lattice gauge theories by dissipation

Tobias Schmale[1,*] and Hendrik Weimer[2,1,†]

[1] Institut für Theoretische Physik, Leibniz Universität Hannover, Appelstraße 2, 30167 Hannover, Germany
[2] Institut für Theoretische Physik, Technische Universität Berlin, Hardenbergstraße 36 EW 7-1, 10623 Berlin, Germany

(Dated: April 26, 2024)

Simulations of lattice gauge theories on noisy quantum hardware inherently suffer from violations of the gauge symmetry due to coherent and incoherent errors of the underlying physical system that implements the simulation. These gauge violations cause the simulations to become unphysical requiring the result of the simulation to be discarded. We investigate an active correction scheme that relies on detecting gauge violations locally and subsequently correcting them by dissipatively driving the system back into the physical gauge sector. We show that the correction scheme not only ensures the protection of the gauge symmetry, but it also leads to a longer validity of the simulation results even within the gauge-invariant sector. Finally, we discuss further applications of the scheme such as preparation of the many-body ground state of the simulated system.

arXiv:2404.16454v1 [quant-ph] 25 Apr 2024

The quantum simulation of lattice gauge theories is one of the most important applications of quantum computers, given that the fundamental field theories that govern modern physics are gauge theories. However, error processes in noisy intermediate-scale (NISQ) quantum devices may violate the gauge symmetry that is essential for the viability of the simulation. Here, we show that engineered dissipation can overcome these limitations and protect the validity of the results for much longer simulation times.

The main challenge when implementing a quantum simulation of a lattice gauge theory is that the gauge symmetry has to be explicitly programmed into the device [1–5]. For current NISQ devices, this means that unavoidable errors will generically lead to violations of the gauge symmetry and result in the creation of quantum states that are unphysical simulation results. To solve this problem, several solutions have been offered. One solution is to integrate out the redundant degrees of freedom. This however typically results in non-local interactions [6], increasing the complexity of the simulation. Other approaches include modifications to the Hamiltonian to attribute an energy penalty to a gauge violation [7], adding (random) gauge transformations during time evolution in order to stochastically cancel gauge errors [8, 9] or detecting gauge violations using oracles and rejecting simulations with gauge violations [10].

In our work, we build on the vast work on the realization of engineered dissipation channels for quantum many-body systems [11–25]. Specifically, we detect gauge violations during the time evolution and apply local correction operations in real time to fix any gauge violations that might occur. We investigate the effects of our scheme on the accuracy of simulations and show control over the temperature of the system as an additional benefit of our approach. We exemplify our result for a Z_2 lattice gauge theory, however, generalization of our work to other lattice gauge theories is straightforward.

A. Model gauge theory

For concreteness, we focus on a paradigmatic Z_2 lattice gauge theory as one of the simplest, yet non-trivial lattice gauge theories [26]. The Hamiltonian is of the form

$$H_0 = \sum_{j=1}^{N} \left[J_a(\sigma_j^+ \tau^z_{j,j+1} \sigma^-_{j+1} + \mathrm{h.c.}) - J_f \tau^x_{j,j+1} \right]. \qquad (1)$$

acts on N matter sites, each of which can contain either the vacuum or a hard-core boson. These are described by the Pauli ladder-operators $\sigma^{+/-}$. In between the matter sites j and $j+1$ sit gauge link variables $\tau^{x/z}_{j,j+1}$, represented by Pauli x/z matrices. Therefore, the system can be mapped to $2N$ qubits. Following [26], we use periodic boundary conditions and set the matter-field coupling $J_a = 1$ and the electric field energy $J_f = 0.54$. Gauge-invariance of this Hamiltonian is defined by the Gauge operators

$$G_j = 1 - (-1)^j \tau^x_{j-1,j} \sigma^z_j \tau^x_{j,j+1}, \qquad (2)$$

which satisfy $[H_0, G_j] = [G_j, G_l] = 0\ \forall j, l$. Once initialized in an eigenvalue g_0 of the gauge operators, the time-evolution should therefore not change this eigenvalue.

However, during a simulation of such a lattice gauge theory on a quantum simulator, unitary and non-unitary errors can break gauge invariance, leading to gauge eigenvalues g deviating from the initial g_0. We incorporate these unitary effects by adding a small gauge variant perturbation

$$H_1 = \sum_{j=1}^{N} \left[(\sigma_j^+ (c_1 \tau^-_{j,j+1} + c_2 \tau^+_{j,j+1}) \sigma^-_{j+1} + h.c.) \right] \qquad (3)$$

$$+ \sum_{j=1}^{N} \sigma_j^+ \sigma_j^- (c_3 \tau^z_{j,j+1} + c_4 \tau^z_{j-1,j}) \qquad (4)$$

* tobias.schmale@itp.uni-hannover.de
† weimer@tu-berlin.de

to the Hamiltonian, resulting in the complete Hamiltonian

$$H = H_0 + \lambda H_1. \tag{5}$$

The precise values of the dimensionless coupling constants c_i are not important, in line with previous work we set them to $c_1 = 0.51$, $c_2 = -0.49$, $c_3 = 0.77$, $c_4 = 0.21$ [26]. Incoherent errors are represented by single-site Lindbladian jump operators L_i acting on all matter and link sites, resulting in the model dynamics being described by the Lindblad master equation

$$\dot{\rho} = i[\rho, H] + \sum_i \left[L_i \rho L_i^\dagger - \frac{1}{2}\rho L_i^\dagger L_i - \frac{1}{2} L_i^\dagger L_i \rho \right]. \tag{6}$$

As L_i we investigate bit-flips $\sqrt{\gamma}\sigma^x$ and phase-flips $\sqrt{\gamma}\sigma^z$ on matter and link sites, and alternatively spontaneous emission $\sqrt{\gamma}\sigma^- = \sqrt{\gamma}(\sigma^x - i\sigma^z\sigma^x)$ on all sites.

We quantify the gauge violation by

$$\varepsilon(t) = \frac{1}{N}\left| \sum_{j=1}^{N} \langle G_j(t) \rangle - \sum_{j=1}^{N} \langle G_j(0) \rangle \right| = \frac{1}{N} \sum_{j=1}^{N} \langle G_j(t) \rangle\,, \tag{7}$$

where the last equation holds by the choice of the initial gauge $\langle G_j(0) \rangle = 0 \ \forall j$.

B. Active gauge correction scheme

We imagine the above lattice gauge theory to be simulated in a Trotterized manner on a digital quantum computer, where time-evolution is split into small time-steps, which are implemented by unitary operations [6, 27–29]. After a variable number of time-steps, mid-circuit measurements of all gauge operators can be performed, e.g. using the circuit from Fig. 1, making use of the fact that the gauge operators and the Hamiltonian all mutually commute. [10] shows how to do this for general lattice gauge theories. This yields a sequence of gauge eigenvalues corresponding the each gauge operator $(G_1, ..., G_N)$. We can now react to this measured gauge syndrome and apply unitary operations to restore the original gauge $(G_1, ..., G_N) = (0, ..., 0)$.

In order find a set of possible correction operators, we first study the action of bit-flips and phase flips on the gauge eigenvalue. The gauge operators G_j have two eigenvalues 0 and 2. A bit-flip on matter site j will flip the eigenvalue of G_j. Similarly, a phase-flip on link site j will flip the eigenvalue of the operators G_j and G_{j+1}. On the other hand, bit-flips on link sites and phase-flips on matter sites do not result in a change of the gauge eigenvalue. This is summarized in Table I. It therefore makes sense to separate the errors into *gauge-variant*, i.e. gauge violating errors and the remaining *gauge-invariant* errors.

Error	Gauge eigenvalues G_{j-i}, G_j, G_{j+1}
σ_j^x	0, 2, 0
σ_j^z	0, 0, 0
$\tau_{j,j+1}^x$	0, 0, 0
$\tau_{j,j+1}^z$	0, 2, 2

TABLE I. Summary of how single qubit errors affect the gauge.

Since not all errors are visible to the gauge operators, one can not hope to achieve full error correction from the gauge theory alone. It is possible to extend the lattice gauge theory to a full quantum error correcting code by adding more degrees of freedom and formulating constraints on these [30]. Instead we here investigate phenomena that to not require extra qubit resources.

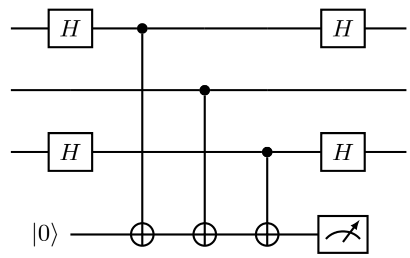

FIG. 1. Circuit for performing the ancilla assisted stabilizer measurement necessary to detect a gauge violation. The three qubits correspond to the three sites that the gauge operator acts on.

The gauge syndromes in Table I suggests the following correction scheme:

- If a sequence $(G_{j-i}, G_j, G_{j+1}) = (0, 2, 0)$ is measured, a correcting bit-flip is applied to matter site j.
- If a sequence $(G_j, G_{j+1}) = (2, 2)$ is measured, a correcting phase-flip is applied to link site j.

In both cases, all gauge eigenvalues are subsequently restored to the physical sector after correction. This scheme could now be applied stroboscopically after a fixed number n of Trotter steps, each evolving the system by time dt, using mid-circuit measurements and real-time feedback [31, 32].
For our numerical simulations, we instead choose a different but equivalent formulation based on jump operators. We define P_j^0 and P_j^2 as the projectors that project into the two eigenvalues 0 and 2 of G_j. In fact, here this means that $P_j^2 = G_j/2$ and $P_j^0 = 1 - P_j^2$. We then define the *correction jump operators* as

$$C_j^x = \sqrt{\gamma_c}\sigma_j^x P_{j-1}^0 P_j^2 P_{j+1}^0 \qquad \text{and} \tag{8}$$

$$C_j^z = \sqrt{\gamma_c}\tau_{j,j+1}^z P_j^2 P_{j+1}^2, \tag{9}$$

which correct the two gauge syndromes given above and annihilate any other sequence of gauge eigenvalues.

$\gamma_c = \frac{1}{n \cdot dt}$ is the *correction rate* and specifies how many correction operations are applied per unit time. We then simulate the dynamics of the correction scheme by using these operators as additional jump operators in the master equation. This is equivalent to the stroboscopic application of the correction circuit since the latter corresponds to a Trotterized form of the master equation dynamics [2].

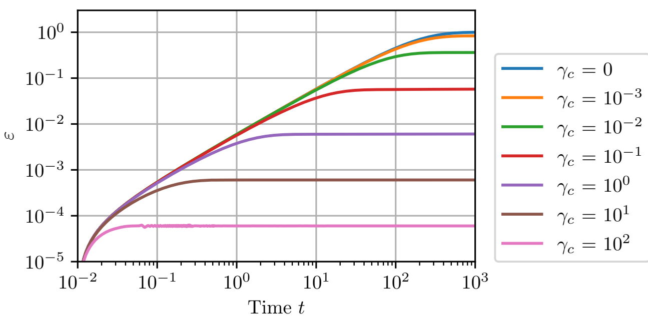

FIG. 2. The gauge violation (7) is tracked over time for different correction rates γ_c, starting from the ground-state ($\lambda = 10^{-2}$, $\gamma = 10^{-3}, N = 4$). Higher correction rates result in smaller gauge violations.

The result of this correction scheme in action can be seen in Figure 2. Without gauge correction ($\gamma_c = 0$), the gauge violation ε increases linearly until a steady-state of maximal gauge violation is reached. Turning on the correction ($\gamma_c > 0$) results in this steady-state violation to be suppressed inversely proportional to the correction rate γ_c. This shows that this scheme is effective in suppressing gauge errors and therefore prevents the simulation of the lattice gauge theory to turn unphysical. We note that since the gauge operators mutually commute, our scheme implements a form of stabilizer pumping [2, 33, 34].

C. Sympathetic cooling during gauge correction

We now make a slight modification to the Hamiltonian by adding the gauge violation as a new term

$$H \to H + g\frac{1}{N}\sum_{j=1}^{N} G_j. \tag{10}$$

This associates an energy penalty g to a gauge violation. We choose $g = 1$ and show a dependence of our results on this choice in the appendix. While such a term can be used to reduce gauge violations stemming from *coherent* errors such as in H_1 [7], they cannot directly suppress *incoherent* errors such as the ones in the master equation (6). However, the combination with our dissipative gauge correction scheme realizes a setup corresponding to a sympathetic cooling of the gauge-invariant sector [35]. Here, the gauge-invariant sector is the system to be cooled, while the gauge degrees of freedom act as a bath. The gauge degrees of freedom are rapidly cooled into the ground state of having no gauge violations, while the coherent gauge errors in Eq. (4) lead to a system-bath coupling and allow energy to be dissipated out of the gauge-invariant sector.

This is similar to the cooling schemes shown in [35] and [36, 37], with the crucial difference that these schemes require extra bath degrees of freedom to be artificially added to achieve cooling, therefore increasing the cost of the simulation. Here, the bath is implemented by the gauge degrees of freedom and does not require any additional resources.

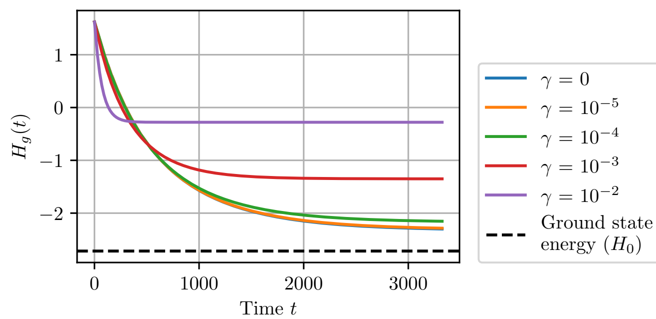

FIG. 3. Cooling is demonstrated by the gauge sector energy (11) decreasing during time evolution. The steady state energy depends on the incoherent error rate γ ($\lambda = 0.1, \gamma_c = 1, N = 3$, σ^- decay).

We show this in Figure 3, where we start in a high-energy product state and demonstrate how the dissipative time-evolution drives the system to lower energy states. To ensure that any energy difference is not a direct consequence of the gauge penalty (10), we only measure the energy of the system in the physical sector as

$$H_g(t) = \frac{\mathrm{Tr}[PH_0P\rho(t)]}{\mathrm{Tr}[P\rho(t)]}, \tag{11}$$

where $P = \prod_j P_j^0$ is the projector into the physical gauge sector. Depending on the magnitude of the competing heating caused by the dissipative errors, an energy close to the ground state can be reached. This final state is then stable under further time evolution, i.e. is protected from further heating. We show this by directly solving for the steady state of the time evolution by computing the eigenvector of the Liouvillian corresponding to the zero-eigenvalue. The results in Figure 4 (lower left) show three distinct phenomena: (i) For low correction rates γ_c, energy is not removed fast enough to compete with heating, hence no significant cooling is achieved. (ii) For too high correction rates, gauge errors are removed too quickly and therefore do not have time to interact with the physical gauge sector by means of the unitary errors. Therefore cooling is also not observed in this "quantum Zeno" regime. (iii) In between these two extremes lies a regime where optimal cooling is achieved. If a gauge error occurs, it has time to interact with the physical sector and a subsequent correction removes its high energy contributions. The steady-state gauge violation ε_{ss} that is achieved scales mostly as $\varepsilon_{ss} \sim \frac{\gamma}{\gamma_c}$, as evident from Fig. 4 (upper left). Exceptions to this rule are regimes of weak correction where the gauge violation saturates as well as intermediate regimes with low incoherent error rates where coherent errors dominate the gauge violation. Remarkably, these results are quite insensitive to the exact nature of the incoherent errors. In Figure 4 (right) we show the same results for spontaneous emission σ^- acting on all matter and link sites and the results still hold. The dependence of these results on the magnitude of coherent errors and the gauge penalty is shown in the appendix.

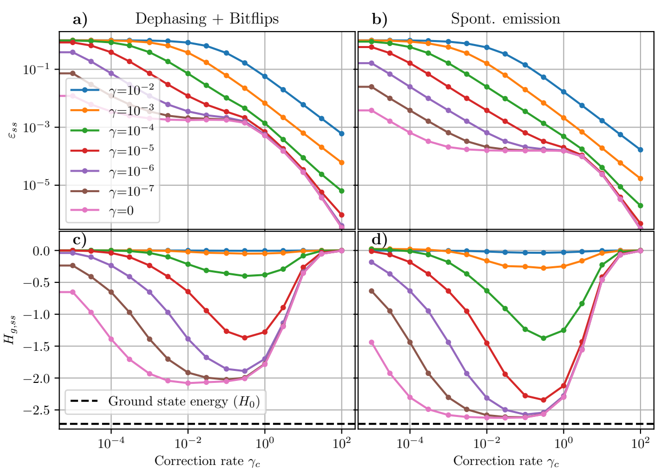

FIG. 4. The steady state gauge violation (**a)** and **b)**) from Eq. (7) and gauge sector energy (**c)** and **d)**) from Eq. (11) is shown for various correction rates γ_c and errors with rate γ on all sites. Maximum cooling is achieved in intermediate correction regimes where correction rates are not too small to be effective and not too large to fall into the Zeno regime, as explained in the main text (**a)** and **c)**: Dephasing and bit-flips on all sites, **b)** and **d)**: Spontaneous emission on all sites, $\lambda = 0.03, N = 3$).

D. Stabilizing quantum simulations

Next, we apply our scheme to increase the accuracy of observables during a simulated time evolution. To this extent, we start the system in a $J_a = 0$ eigenstate and then quench to the previously used $J_a > 0$ and track the dynamics of observables over time. Figure 5 show the trajectory of the observable

$$O = \sum_j \tau^x_{j-1,j}\tau^x_{j,j+1}, \tag{12}$$

i.e. a link-link correlator. In the appendix, we show results for more observables. The lower panels show the deviation of the observable from the exact, noise-free dynamics. This deviation is time-averaged over a running window of 10 time units for improved legibility.

We first focus on gauge-variant errors, i.e., bit-flips on matter sites and phase-flips on link sites. Since bit and phase errors can be exchanged by a local unitary transformation, this scenario is equivalent to the case where only bit or phase errors occur on all sites. Experimental platforms where one type of error dominates over the other are quite common, ranging from trapped ions [38, 39] to solid-state spin qubits [40].

As incoherent gauge-variant errors are localized single-qubit errors, their presence causes in correlations to quickly decay to zero if no correction is present, while the noise free evolution shows interesting dynamics even for long times. As evident from Fig. 5 (lower left), turning on the gauge corrections restores these dynamics and prevents a decay of the correlators. In this scenario with only gauge-invariant errors, the gauge corrections represent a full error correction of individual errors, as every error is visible as a gauge violation and can uniquely be decoded and corrected. We note that this works most reliably if the correction rate is faster than the timescale of the Hamiltonian to be simulated. However, this is guaranteed in digital quantum simulation approaches where the individual parts of the Hamiltonian are implemented in a Trotterized form and the correction is carried out after each Trotter step.

If we also turn on the gauge-invariant errors, the protective effect of the correction is reduced, but does not vanish entirely. The corrected dynamics still show reduced errors as compared to the uncorrected ones. Since only the gauge-variant errors can be corrected, one may assume the simulation to be similar to an uncorrected simulation with only gauge-invariant errors. The effect of the correction is therefore to reduce the magnitude of the incoherent errors.

While sympathetic cooling requires moderate coherent errors λ and comparatively small correction rates γ_c, stabilizing time evolution does not require coherent errors but higher correction rates. Hence λ and γ_c are the crucial parameters that govern which of the two regimes are explored. Depending of the desired use-case, the coherent errors are either a result of simulation errors, or can be artificially added to engineer the cooling effect. Hence it is possible to tune both parameters to achieve the desired application.

E. Discussion

We have demonstrated that an active error correction scheme can successfully suppress gauge errors in lattice gauge theory simulations, inversely proportional to the correction rate. We showed how this gauge correction scheme can be interpreted as a sympathetic cooling setup and showed that this allows for tuning the parameters to the point where even ground states can be prepared and

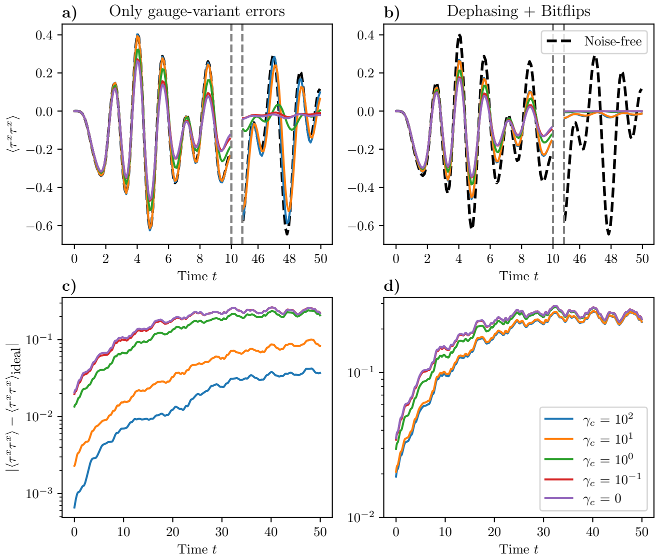

FIG. 5. **a)** and **b)**: The link-link correlator (12) is shown as a function of time for various correction rates γ_c. Without correction, the correlator decays, but the noise free dynamics can be restored by the correction scheme. **c)** and **d)**: Deviation from the noise free dynamics, time-averaged across 10 time units for improved legibility. ($\lambda = 0.04, \gamma = 0.01, N = 4$).

stabilized. This cooling scheme is very robust and its effects can be seen no matter the exact structure of the coherent errors, incoherent errors or the nature of the correction scheme. Our results can be directly applied to efforts to simulate lattice gauge theory on present NISQ devices [41]. Finally we showed that this scheme can increase the accuracy of observables during simulation and therefore acts like a precursor to error correction. It is particularly suitable in situations where errors are anisotropic as the scheme turns into full error correction in this case. However even without assumptions about the structure of the error, the scheme allows steady states of observables to be estimated more accurately.

[1] S. Tewari, V. W. Scarola, T. Senthil, and S. D. Sarma, Emergence of artificial photons in an optical lattice, Phys. Rev. Lett. **97**, 200401 (2006).
[2] H. Weimer, M. Müller, I. Lesanovsky, P. Zoller, and H. P. Büchler, A rydberg quantum simulator, Nature Phys. **6**, 382 (2010).
[3] U.-J. Wiese, Ultracold quantum gases and lattice systems: quantum simulation of lattice gauge theories, Annalen der Physik **525**, 777 (2013).
[4] K. Stannigel, P. Hauke, D. Marcos, M. Hafezi, S. Diehl, M. Dalmonte, and P. Zoller, Constrained dynamics via the zeno effect in quantum simulation: Implementing non-abelian lattice gauge theories with cold atoms, Phys. Rev. Lett. **112**, 120406 (2014).
[5] M. Dalmonte and S. Montangero, Lattice gauge theory simulations in the quantum information era, Contemporary Physics **57**, 388 (2016).
[6] E. A. Martinez, C. A. Muschik, P. Schindler, D. Nigg, A. Erhard, M. Heyl, P. Hauke, M. Dalmonte, T. Monz, P. Zoller, and R. Blatt, Real-time dynamics of lattice gauge theories with a few-qubit quantum computer, Nature **534**, 516 (2016).
[7] J. C. Halimeh, H. Lang, J. Mildenberger, Z. Jiang, and P. Hauke, Gauge-symmetry protection using single-body terms, PRX Quantum **2**, 040311 (2021).
[8] M. C. Tran, Y. Su, D. Carney, and J. M. Taylor, Faster digital quantum simulation by symmetry protection, PRX Quantum **2**, 010323 (2021).
[9] H. Lamm, S. Lawrence, and Y. Yamauchi, Suppressing coherent gauge drift in quantum simulations (2020), 2005.12688 [hep-lat, physics:quant-ph].
[10] J. R. Stryker, Oracles for gauss's law on digital quantum computers, Physical Review A **99**, 042301 (2019).
[11] S. Diehl, A. Micheli, A. Kantian, B. Kraus, H. P. Büchler, and P. Zoller, Quantum states and phases in driven open quantum systems with cold atoms, Nature Physics **4**, 878 (2008).
[12] F. Verstraete, M. M. Wolf, and J. Ignacio Cirac, Quantum computation and quantum-state engineering driven by dissipation, Nature Phys. **5**, 633 (2009).
[13] J. T. Barreiro, M. Müller, P. Schindler, D. Nigg, T. Monz, M. Chwalla, M. Hennrich, C. F. Roos, P. Zoller, and R. Blatt, An open-system quantum simulator with trapped ions, Nature **470**, 486 (2011).
[14] H. Krauter, C. A. Muschik, K. Jensen, W. Wasilewski, J. M. Petersen, J. I. Cirac, and E. S. Polzik, Entanglement generated by dissipation and steady state entanglement of two macroscopic objects, Phys. Rev. Lett. **107**, 080503 (2011).
[15] A. W. Carr and M. Saffman, Preparation of entangled and antiferromagnetic states by dissipative rydberg pumping, Phys. Rev. Lett. **111**, 033607 (2013).
[16] D. D. B. Rao and K. Mølmer, Dark entangled steady states of interacting rydberg atoms, Phys. Rev. Lett. **111**, 033606 (2013).
[17] Y. Lin, J. P. Gaebler, F. Reiter, T. R. Tan, R. Bowler, A. S. Sørensen, D. Leibfried, and D. J. Wineland, Dissipative production of a maximally entangled steady state of two quantum bits, Nature **504**, 415 (2013), arXiv:1307.4443 [quant-ph].
[18] S. Shankar, M. Hatridge, Z. Leghtas, K. M. Sliwa, A. Narla, U. Vool, S. M. Girvin, L. Frunzio, M. Mir-

rahimi, and M. H. Devoret, Autonomously stabilized entanglement between two superconducting quantum bits, Nature **504**, 419 (2013), arXiv:1307.4349 [quant-ph].
[19] G. Morigi, J. Eschner, C. Cormick, Y. Lin, D. Leibfried, and D. J. Wineland, Dissipative quantum control of a spin chain, Phys. Rev. Lett. **115**, 200502 (2015).
[20] F. Reiter, D. Reeb, and A. S. Sørensen, Scalable dissipative preparation of many-body entanglement, Phys. Rev. Lett. **117**, 040501 (2016).
[21] H. Weimer, Tailored jump operators for purely dissipative quantum magnetism, J. Phys. B **50**, 024001 (2017).
[22] M. Roghani and H. Weimer, Dissipative preparation of entangled many-body states with rydberg atoms, Quantum Sci. Technol. **3**, 035002 (2018).
[23] M. Metcalf, J. E. Moussa, W. A. de Jong, and M. Sarovar, Engineered thermalization and cooling of quantum many-body systems, Phys. Rev. Research **2**, 023214 (2020).
[24] A. Jamadagni, S. Ospelkaus, L. Santos, and H. Weimer, Quantum zeno-based detection and state engineering of ultracold polar molecules, Phys. Rev. Research **3**, 033208 (2021).
[25] L. Piroli, G. Styliaris, and J. I. Cirac, Quantum circuits assisted by local operations and classical communication: Transformations and phases of matter, Phys. Rev. Lett. **127**, 220503 (2021).
[26] J. C. Halimeh, V. Kasper, and P. Hauke, Fate of lattice gauge theories under decoherence, arXiv:2009.07848 [cond-mat, physics:hep-lat, physics:quant-ph] (2020), 2009.07848.
[27] S. Lloyd, Universal Quantum Simulators, Science **273**, 1073 (1996).
[28] A. Smith, M. S. Kim, F. Pollmann, and J. Knolle, Simulating quantum many-body dynamics on a current digital quantum computer, npj Quantum Information **5**, 106 (2019).
[29] B. Fauseweh, Quantum many-body simulations on digital quantum computers: State-of-the-art and future challenges, Nature Communications **15**, 2123 (2024).
[30] A. Rajput, A. Roggero, and N. Wiebe, Quantum error correction with gauge symmetries, npj Quantum Information **9**, 41 (2023).
[31] J. M. Koh, S.-N. Sun, M. Motta, and A. J. Minnich, Measurement-induced entanglement phase transition on a superconducting quantum processor with mid-circuit readout, Nature Physics **19**, 1314 (2023).
[32] T. Schmale, B. Temesi, N. Trittschanke, N. Pulido-Mateo, I. Elenskiy, L. Krinner, T. Dubielzig, C. Ospelkaus, H. Weimer, and D. Borcherding, Real-time hybrid quantum-classical computations for trapped ions with python control-flow, in *2023 IEEE International Conference on Quantum Software (QSW)* (IEEE, 2023) pp. 193–199.
[33] H. Weimer, M. Müller, H. P. Büchler, and I. Lesanovsky, Digital quantum simulation with rydberg atoms, Quant. Inf. Proc. **10**, 885 (2011).
[34] M. Müller, K. Hammerer, Y. L. Zhou, C. F. Roos, and P. Zoller, Simulating open quantum systems: from many-body interactions to stabilizer pumping, New Journal of Physics **13**, 085007 (2011).
[35] M. Raghunandan, F. Wolf, C. Ospelkaus, P. O. Schmidt, and H. Weimer, Initialization of quantum simulators by sympathetic cooling, Science Advances **6**, eaaw9268 (2020).
[36] S. Polla, Y. Herasymenko, and T. E. O'Brien, Quantum digital cooling, Physical Review A **104**, 012414 (2021).
[37] X. Mi *et al.*, Stable quantum-correlated many-body states through engineered dissipation, Science **383**, 1332 (2024).
[38] T. Ruster, C. T. Schmiegelow, H. Kaufmann, C. Warschburger, F. Schmidt-Kaler, and U. G. Poschinger, A long-lived zeeman trapped-ion qubit, Applied Physics B **122**, 254 (2016).
[39] H. H. Vallabhapurapu, I. Hansen, C. Adambukulam, R. Stöhr, A. Denisenko, C. H. Yang, and A. Laucht, High-fidelity control of a nitrogen-vacancy-center spin qubit at room temperature using the sinusoidally modulated, always rotating, and tailored protocol, Physical Review A **108**, 022606 (2023).
[40] H. Weimer, N. Y. Yao, and M. D. Lukin, Collectively enhanced interactions in solid-state spin qubits, Physical Review Letters **110**, 067601 (2013).
[41] T. Angelides, P. Naredi, A. Crippa, K. Jansen, S. Kühn, I. Tavernelli, and D. S. Wang, First-Order Phase Transition of the Schwinger Model with a Quantum Computer, arXiv e-prints , arXiv:2312.12831 (2023), arXiv:2312.12831 [hep-lat].
[42] J. Johansson, P. Nation, and F. Nori, QuTiP 2: A python framework for the dynamics of open quantum systems, Comput. Phys. Commun. **184**, 1234 (2013).

ACKNOWLEDGMENTS

Master-equation time-evolution trajectories and steady-state computations were computed using the QUTIP library [42]. This work was funded by the Quantum Valley Lower Saxony (QVLS) through the Volkswagen foundation and the ministry for science and culture of Lower Saxony and by Germany's Excellence Strategy – EXC-2123 QuantumFrontiers – 390837967.

COMPETING INTERESTS

The authors declare no competing interests.

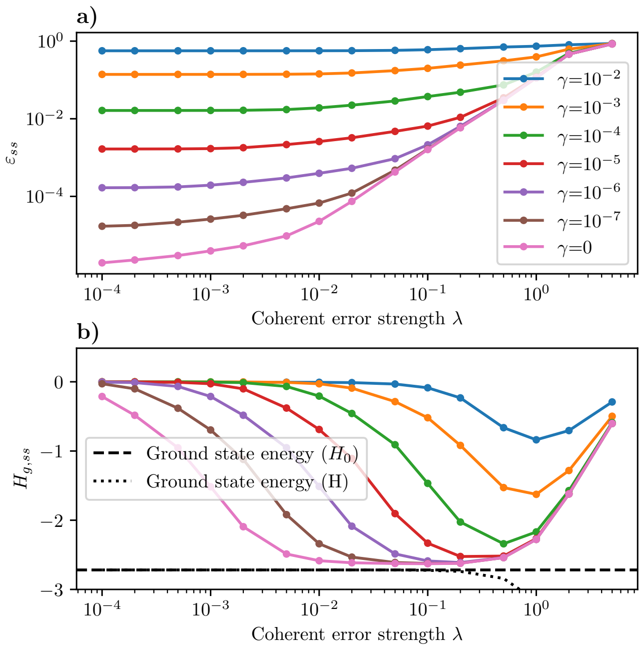

FIG. 6. **a)** The steady state gauge violation (7) and **b)** gauge sector energy (11) is shown for varying coherent error magnitudes λ and spontaneous emission with rate γ on all sites. ($\gamma_c = 0.01, N = 3$).

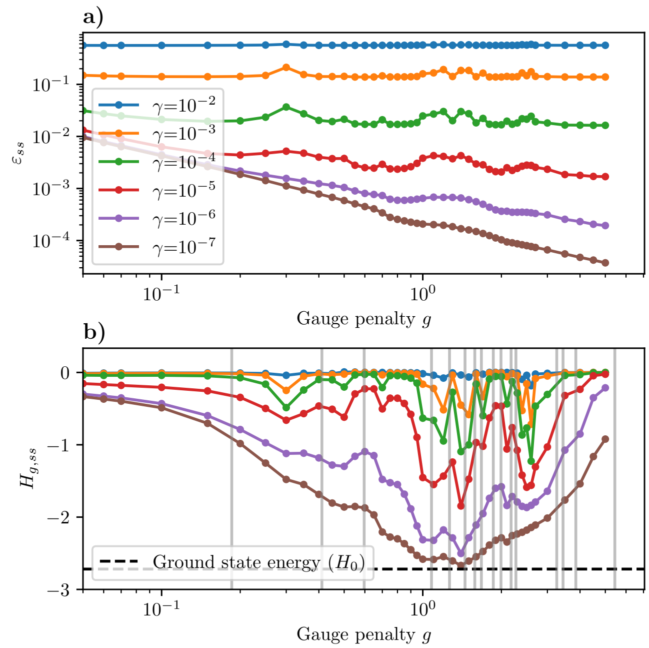

FIG. 7. **a)** The steady state gauge violation (7) and **b)** gauge sector energy (11) is shown for gauge penalties g and spontaneous emission with rate γ on all sites. Vertical gray lines indicate energy transitions in the system Hamiltonian. ($\gamma_c = 0.01, N = 3$).

Appendix A: Parameter dependencies of steady state results

Fig. 6 shows the dependence of the achieved cooling on the magnitude of the coherent errors. Stronger decoherence requires more coherent errors, at the cost of a larger steady-state gauge violation. For smaller decoherence rates, the system is not sensitive to the exact value of the coherent error magnitude. In Figure 7 we also show the dependence of the cooling results on the gauge penalty g. The best cooling is achieved when the gauge penalty lies in a region with many energy transitions of H_0 [35]. The steady-state gauge violations here recover the known result that the gauge penalty alone can yield a gauge-correcting effect [7] if only unitary errors are present.

Appendix B: Matter-matter correlations

In special cases, the steady-error of observables may even be reduced by the correction scheme as shown in Fig. 8, where a matter-matter correlator is tracked over time. As with the previous results, gauge-variant errors can be fully corrected. In contrast to the result in the main text, the long-term behavior of the uncorrected results starts to significantly deviate from the true solution, while the errors of the corrected simulations remain bounded.

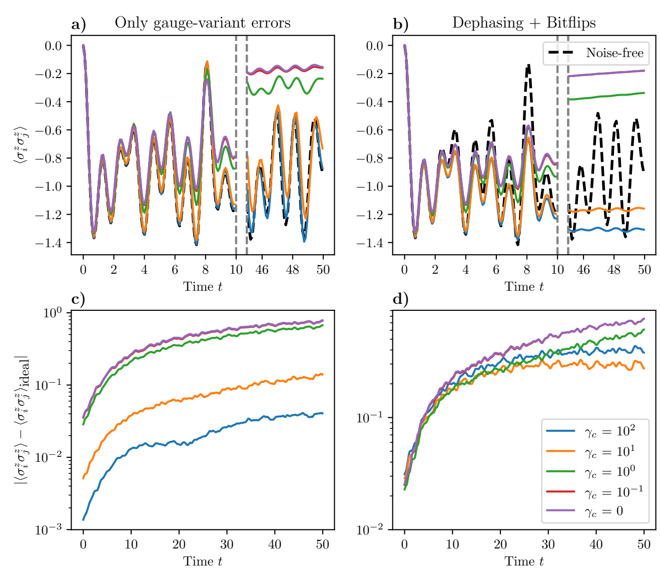

FIG. 8. **a)** and **b)**: Matter-matter correlator is shown as a function of time for various correction rates γ_c. Without correction, the correlator decays, but the noise free dynamics can be restored by the correction scheme. **c)** and **d)**: Deviation from the noise free dynamics, time-averaged across 10 time units for improved legibility ($\lambda = 0.04, \gamma = 0.01, N = 4$).